


Flash graphene from carbon fiber composites: A sustainable and high-performance electrocatalyst for hydrogen peroxide production

Ivo Bardarov^{a,b}, Desislava Yordanova Apostolova^a, Pedro Martins^b, Ivo Angelov^c, Francisco Ruiz-Zepeda^b, Ivan Jerman^b, Matevž Dular^d, Dušan Strmčnik^b, Boštjan Genorio^{a,*} 

^a Faculty of Chemistry and Chemical Technology, University of Ljubljana, Večna pot 113 1000, Ljubljana, Slovenia

^b Department of Materials Chemistry, National Institute of Chemistry, Hajdrihova 19 1001, Ljubljana, Slovenia

^c Faculty of Engineering, South-West University "Neofit Rilski", Ivan Mihaylov Str. 66 2700, Blagoevgrad, Bulgaria

^d Faculty of Mechanical Engineering, University of Ljubljana, Aškerčeva cesta 6 1000, Ljubljana, Slovenia

ARTICLE INFO

Keywords:

Flash graphene
Flash Joule heating
Carbon fiber composite
Carbon materials
Hydrogen peroxide
Electrochemical synthesis
Upcycling, Sustainability

ABSTRACT

Carbon fiber-reinforced polymer (CFRP) composites are indispensable in various industries due to their exceptional strength-to-weight ratio, outstanding durability, and high stiffness. However, the effective recycling of CFRP remains a major challenge and requires the development of advanced technologies and more sustainable waste management solutions. In this study, we present an efficient and reproducible method for upcycling CFRP waste into large quantities of carbon fiber composite flash graphene (CFC-FG) by cost-effective flash Joule heating (FJH) in the millisecond range. The resulting flash graphene was extensively characterized by morphological, structural, spectroscopic, and chemical analyses. These investigations revealed a highly porous, lamellar structure with a low concentration of oxygen functional groups and a turbostratic graphitic structure. Important structural features, including a distinct D' peak in Raman spectra and elliptical ring patterns observed in selected area electron diffraction (SAED), emphasized its unique properties. These combined attributes of CFC-FG resulted in excellent electrochemical performance in the two-electron oxygen reduction reaction ($2e^-$ ORR) for the electrosynthesis of hydrogen peroxide (H_2O_2). CFC-FG showed nearly 100 % selectivity and good activity in 0.1 M KOH, with stability tests confirming the retention of performance, making it a promising candidate for real electrosynthesis applications. The core concept of this work was to develop a recycled, sustainable electrocatalyst for H_2O_2 electrosynthesis that contributes to a circular economy and supports global sustainability goals.

1. Introduction

Hydrogen peroxide (H_2O_2) is a powerful and versatile environmentally friendly oxidizing agent. It is one of the most important common chemicals in the world with an annual market size of USD 3.3 billion in 2023, which is expected to grow and reach USD 4.5 billion by 2032 [1]. Today, more than 95 % of the world's H_2O_2 is produced by the energy and waste-intensive centralized multi-step anthraquinone process, which requires organic solvents and Pd catalysts [2]. A cleaner and more sustainable alternative is the direct electrochemical synthesis of H_2O_2 from water and oxygen by the two-electron oxygen reduction reaction ($2e^-$ ORR). This process has gained significant attention due to its ability to produce H_2O_2 on-site and on-demand [3]. It also eliminates the need for costly transportation of the hazardous H_2O_2 and the required

concentration-dilution steps. The main obstacle to the commercialization of the electrochemical synthesis of H_2O_2 through the $2e^-$ ORR is the lack of efficient and selective catalysts. Various catalysts have been demonstrated to facilitate the process with limited efficiency. Among them, platinum group metals (PGM) and their alloys, such as Pd–Hg [4], Au–Pd [5], are currently the most active and stable, with overpotentials close to zero and H_2O_2 selectivity up to 98 %. However, the scarcity and high price of PGM hinder their extensive adoption. Transition metal catalysts such as Co [6], Fe [7], and Ni [8] also show good overall performance but are prone to poisoning and deactivation by impurities in the electrolyte. This underlines the potential of carbon nanomaterials, which have been shown to be effective and selective electrocatalysts for $2e^-$ ORR applications. There was a demonstration of the application of active oxidized carbon materials in H_2O_2 electrosynthesis [9].

* Corresponding author.

E-mail address: bostjan.genorio@fkkt.uni-lj.si (B. Genorio).

<https://doi.org/10.1016/j.electacta.2025.145754>

Received 5 December 2024; Received in revised form 15 January 2025; Accepted 25 January 2025

Available online 26 January 2025

0013-4686/© 2025 The Author(s). Published by Elsevier Ltd. This is an open access article under the CC BY license (<http://creativecommons.org/licenses/by/4.0/>).

Researchers also reported the use of heteroatom-doped graphene-based materials, and defect-doped graphene, all of which can significantly improve $2e^-$ ORR performance for H_2O_2 electrosynthesis but are still inferior compared to metal electrocatalysts [10–14]. Many reported carbon electrocatalysts involve complex and time-consuming synthesis processes, making them less appealing for commercial applications. Aligning with green initiatives, it would be highly advantageous to use recycled or upcycled waste materials as precursors for electrocatalysts, promoting sustainability and reducing environmental impact. Examples of such precursor materials include carbon fiber-reinforced polymers (CFRPs) and carbon fiber composites (CFCs). Their remarkable strength-to-weight and stiffness-to-weight ratios, electrical conductivity, good fatigue, and corrosion resistance make them indispensable materials in various sectors, including renewable energy. In 2021, the production of wind turbine blades alone consumed 50.8×10^6 kg of CFRP, representing 28 % of total global demand. The demand for CFRP has grown steadily since its first commercial application in the early 1970s. The size of the CFRP market is estimated to reach USD 39.412 billion by 2033, almost double that of 2023 [15,16]. This growth raises awareness of the impact of these materials on the environment at the end of a product's life. Recycling and reuse are the naturally best choices, however, there are considerable difficulties in recycling [17, 18]. CFRP waste comes not only from end-of-life (EoL) products, but also from out-of-date pre-pregs, manufacturing cut-offs, testing materials production tools, etc. [19,20]. Manufacturing waste accounts for around 40 % of all CFRP waste [21]. Landfilling and incineration have long been the predominant methods of treating composite waste [22,23]. Although much research has been done in the field of CFRP waste recycling over the last two decades, still a significant amount of CFRP's end up in landfills [18,24,25]. An advantageous solution for the management of such waste is to transform it into high-value carbon materials. The fibers are nearly 100 % carbon, and the epoxy resins and polymers used as binders can be efficiently transformed into substantial quantities of carbon through pyrolysis. This makes CFC waste an ideal precursor for upcycling into carbon nanomaterials, such as graphene, which can be utilized in electrocatalysis applications.

Since its discovery in 2004, graphene has sparked a revolutionary transformation in materials science, emerging as the most promising substance of the 21st century. Its potential has drawn extensive attention from both researchers and industry, generating significant innovations across various fields [26,27]. Nevertheless, its wide-scale commercial applications are still hindered mainly because traditional methods for obtaining graphene still face drawbacks such as high cost, complicated scalability, sustainability concerns related to the environmental impact, or low quality of the product [28]. A significant step towards overcoming these drawbacks was taken in 2019 by Tour and co-workers, who converted various carbon sources into bulk quantities of turbostratic flash graphene (FG) by flash Joule heating (FJH) [29].

FJH is a simple and inexpensive bottom-up method for the production of graphene, based on the passage of a rapid burst of electrical current through a conductive sample. As a result of the Joule heat generated inside the carbon material, the temperature of the sample rises to over 3000 K within milliseconds. At this temperature, nonmetals are more volatile than carbon and get removed from the system by outgassing resulting in a carbon product with purity reaching up to 99 wt.%. After the end of the electrical pulse, the sample cools down ultrafast by thermal radiation [30]. Such a process is kinetically controlled. The rapid cooling prevents the carbon sheets from arranging and stacking in the thermodynamically favored Bernal AB-stacked form [28]. The resulting rotational disorder or mismatching leads to weaker Van der Waals interactions between the sheets and increased interlayer spacing. Due to the decreased contribution of $\pi-\pi$ stacking interactions, turbostratic flash graphene can be exfoliated and dispersed into single sheets much more easily compared to AB-stacked graphite [31]. This improves the material's processability for various applications, particularly in the field of electrochemistry. Notably, due to its high

conductivity and tunable properties, FG can also serve as an effective electrocatalyst. Wyss and colleagues synthesized highly porous, holey, and wrinkled flash graphene from mixed plastic waste by in situ salt decomposition. The resulting product exhibited a surface area of up to $874 \text{ m}^2 \text{ g}^{-1}$ and was effectively used as a metal-free HER electrocatalyst and anode material for lithium-metal batteries [32]. In another study, the feasibility of FJH for the facile synthesis of heteroatom-doped FG was demonstrated. Seven elements were used to produce single-atom doped FG as well as two- and three-element co-doped graphene. These materials were used as catalysts for electrochemical oxygen reduction reactions (ORR) and as electrode materials in lithium metal batteries [33,34].

In this article, we present a novel method for upcycling carbon fiber-reinforced polymer (CFRP) into high-quality flash graphene (FG) using flash Joule heating (FJH). The resulting FG exhibits exceptional properties as an electrocatalyst and is highly active, stable, and selective for the electrochemical synthesis of H_2O_2 . This approach not only provides a sustainable solution for the recycling of CFRP waste but also offers a route to the production of advanced materials with significant potential for sustainable energy and chemical applications.

2. Materials and methods

2.1. Synthesis of flash graphene (FG)

Flash graphene was synthesized from industrial cut-offs and expired carbon fiber felt pre-impregnated with epoxy resin (pre-preg - CP012, C-M-P GmbH, Germany), which contains 36 wt.% resin according to the manufacturer. The high electrical conductivity of the carbon fiber component makes these materials particularly suitable for flash Joule heating (FJH), eliminating the need for additional conductive fillers often used in the processes. A custom-made laboratory scale flash Joule heating (FJH) system was built and designed to produce <1g batches of Flash graphene. For safety reasons, the experimental setup was housed in a grounded metal box placed inside a well-ventilated fume hood. The control module including the charging unit and an emergency discharge circuit were placed several meters away from the fume hood to protect the operator. Synthesis is always performed with the sash window closed and proper light protection applied. A voltmeter and a signal light were used to make sure the capacitor bank was fully discharged before samples were collected. A simple schematic diagram of the FJH setup is shown in **Figure S1**. The system features a 168 mF capacitor bank with a nominal voltage of 400 V, charged directly from the mains via a half-wave rectifier and a current-limiting resistor. Current is delivered to the sample through a thyristor switch capable of handling pulse currents up to 16 kA for 10 ms. The duration of the discharge pulse is controlled by an Arduino microcontroller, while an oscilloscope, connected to a computer, monitors both voltage and current in real time throughout the flashing process. Additionally, a 12 VAC power supply rated at 20+ amps is used to pretreat or degas the sample before flashing. This step helps to gradually remove volatiles and gases that could otherwise build up pressure and cause the glass tube containing the sample to burst.

In the standard procedure, 80 mg of raw material is processed into FG with an approximate yield of 50 %. The weight loss is primarily attributed to the generation of a substantial amount of volatile compounds during the pretreatment stage, as well as the ejection of some carbon particles from the sample tube during the flashing process. For detailed information about the setup and operation of the device, see Supplementary Materials (Page 1).

2.2. Electrode preparation and assembly

For electrochemical measuring of the CFC-FG and GC electrocatalysts, an RRDE electrode (AFE6R2GCAU, Pine Research Instrumentation, Inc.) equipped with a fixed GC disk (area = 0.2376 cm^2) and gold ring (area = 0.2356 cm^2) was used. Prior to measurements, the

RRDE electrode was polished using 9 μm and 0.05 μm diamond paste (MetaDiTM Supreme, Buehler), followed by rinsing with copious amount of ultrapure water (resistivity of 18.2 M Ω cm, Milli-Q system). The freshly polished electrode was used for measuring the GC disk. Due to the high purity of the FG produced, no post-treatment was required so that the material could be used directly for the preparation of catalyst suspension (ink) as follows: catalyst suspension with a concentration of 2.376 mg_{catalyst} mL⁻¹ was prepared by mixing 15.6 mg of CFC-FG powder sample with 6.57 mL ultrapure water, 1.31 mL 2-propanol (IPA) (electronic grade, 99.999 % trace metal basis, Sigma-Aldrich) and 56.16 μL perfluorosulfonic acid (PFSA) ionomer dispersion (Aquivion D98–25BS, 25 % in water, PFSA eq. wt. 980 g/mole SO₃H, Sigma-Aldrich). The prepared suspension was then homogenized using a sonicating bath for 1 h. An aliquot of 10 μL was pipetted on the GC disk surface (catalyst loading of 100 $\mu\text{g}_{\text{catalyst}} \text{cm}^{-2}$) and let dry at ambient conditions to obtain a thin film. For the HOPG sample, a custom-made RRDE electrode equipped with a HOPG disk (area = 0.302 cm²), and a platinum ring (area = 0.283 cm²) was used. Before the electrochemical measurements, the HOPG surface was freshly cleaved using adhesive tape. RRDE experiments were performed using a rotator (WaveVortex10, Pine Research Instrumentation, Inc.) and a bi-potentiostat (PalmSens4). The electrochemical cell consisted of an Ag/AgCl/3 M NaCl (BASi Research) as a reference electrode and glassy carbon rod (SIGRADUR®G glassy carbon, HTW Hochtemperatur-Werkstoffe GmbH) as a counter electrode and 0.1 M KOH (KOH hydrate, 99.995 % Suprapur, Supelco, Merck KGaA) as electrolyte. The collection efficiency (N) for Au ring ($N = 0.37$) and Pt ring ($N = 0.20$) were measured ahead of the experiments using 10 mM [Fe(CN)₆]³⁻ in 0.1 M KOH at a rotation speed of 1600 rpm and 50 mV s⁻¹ scan rate.

2.3. Scanning Electron Microscopy (SEM) and Transmission Electron Microscopy (TEM) analysis

The morphology of the materials was examined using a Zeiss ULTRA Plus field emission scanning electron microscope (FE-SEM). The samples were mounted on a conductive carbon tape, placed on an aluminum SEM holder. The SEM images were recorded at 2 kV with an SE2 detector at a working distance (WD) of 5.5 mm. The transmission electron microscopy (TEM) analysis of CFC-FG was performed with a JEOL ARM 200 CF transmission electron microscope operating at an accelerating voltage of 80 kV. The sample was prepared by dispersing the flash graphene on a copper grid coated with a thin carbon film.

2.4. X-ray photoelectron spectroscopy (XPS)

X-ray photoelectron spectroscopy (XPS) measurements were conducted using a Versa Probe 3 AD (PHI, Chanhassen, USA) equipped with a monochromatic Al $K\alpha$ X-ray source. The source operated at an accelerating voltage of 15 kV and an emission current of 13.3 mA. Powder samples were mounted on double-sided Scotch tape and positioned at the center of the XPS holder. Spectra were acquired for each sample over a 1 × 1 mm analysis area, with the charge neutralizer activated during data collection. Survey spectra were measured using a pass energy of 224 eV and a step size of 0.8 eV. High-resolution (HR) spectra were recorded with a pass energy of 27 eV and a step size of 0.1 eV. To ensure high-quality spectral data with a good signal-to-noise ratio, at least 10 sweeps were performed for each measurement. The energy scale of the XPS spectra and any possible charging effects were corrected by referencing the C=C peak in the C 1s spectrum of the carbon support, with a binding energy (BE) of 284.5 eV. Spectral deconvolution was carried out using MultiPak 9.9.1 and CasaXPS software. Shirley background correction was applied to all spectra.

2.5. XRD analysis

The powder X-ray diffraction (XRD) measurements of materials were

carried out on a PANalytical X'Pert PRO MPD diffractometer with Cu $K\alpha 1$ radiation ($\lambda = 1.5406 \text{ \AA}$) in the 2θ range from 10° to 60° with the 0.034° step per 100 s using fully opened X'Celerator detector. Samples were prepared on a zero-background Si holder.

2.6. Raman characterization

Raman spectra were collected using a WITec Alpha 300 RAS system, equipped with a 532 nm laser (5 mW power), a 50 × 0.8 NA objective, and an integration time of 1 s. All spectra are reported as average spectra obtained by large area mapping of 50 μm by 40 μm (100 × 80 pixels).

2.7. BET analysis and particle size distribution (PSD)

The specific surface area and porosity were determined using the Brunauer–Emmett–Teller (BET) method, with nitrogen adsorption at 77 K on a Micromeritics ASAP 2020. Samples were degassed under vacuum at 120 °C for 2 h. Particle Size Analysis: Particle size distribution analysis was performed in wet conditions (aqueous dispersion) using a Microtrac S3500 Bluewave laser particle size analyzer equipped with tri-laser technology.

2.8. TGA analysis

Thermogravimetric measurements were performed on a Netzsch 449 F3 Jupiter (Selb – Germany), instrument under a dynamic Ar (5.0) or Ar/O₂ (80/20 vol. %) flow with a flow rate of 50 mL min⁻¹ in a temperature range from 30 °C to 1200 °C. A heating rate of 10 K min⁻¹ was used. About 15 mg of the sample was placed in a 0.3 mL Al₂O₃ crucible.

2.9. High speed footage

Phantom High-Speed camera (FASTCAM MINI UX100 - Photron, Japan) was used to capture video of the sample during both the pre-heating and FJH.

3. Results and discussion

3.1. Synthesis and characterization

Carbon fiber composite flash graphene (CFC-FG) was synthesized in two steps using the preheating and the flash Joule heating (FJH), as shown in schematics in Fig. 1 (a). To achieve optimal material properties, the process was carefully optimized. In the first step, we focused on the pretreatment of the carbon fiber felt pre-impregnated with epoxy resin (CFC). The pretreatment consisted of resistance heating at 10 A for 10 s. This heating process was uniform, as confirmed by the high-speed video recording screenshot shown in Fig. 1 (b). During the pretreatment, the decomposition of the epoxy resin produces volatiles, which condense on the surface of the electrode holders. After pretreatment in the second step, flash heating was performed for 200 ms with a current reaching 400 A. Interestingly, the screenshot of the high-speed video in Fig. 1 (c) shows inhomogeneous heating during the flash phase. To enhance the understanding of the flash process, a high-speed camera was used to capture video footage of the process (see high-speed video SV1 in the Supplementary Materials). Several studies provide mathematical models and simulations of Joule heating and temperature distribution during FJH [35–37]. These studies consistently show heat accumulation at the center of the sample and lower temperatures near the ends due to heat dissipation through the electrodes [36–38]. However, our findings indicate that this pattern holds only when low currents are applied over extended periods, such as during pretreatment (Fig. 1 (b)). As shown in high-speed video SV1, when the high-voltage pulse is introduced, regions of lower conductivity led to localized overheating evident by the intense light emitted. These hot zones expand and eventually propagate throughout the entire sample. After the electric pulse ends, the sample

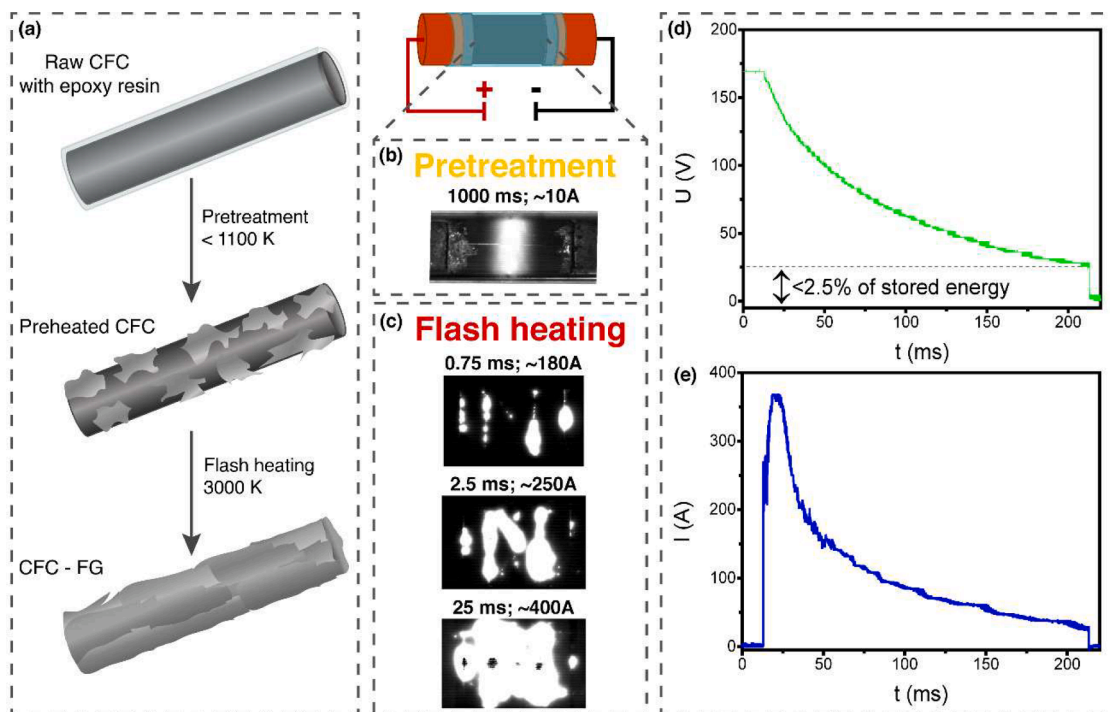


Fig. 1. (a) Schematics of carbon fiber composite flash graphene (CFC-FG) synthesis in two steps. The first step involves the pretreatment pyrolysis of epoxy resin, followed by the second step, which is flash Joule heating (FJH), resulting in the production of CFC-FG. (b) High-speed video screenshot of pretreatment, and (c) High-speed video screenshots of FJH at different time frames. (d) Voltage discharge of capacitor bank during FJH, (e) Electrical current flow through the sample during FJH pulse.

rapidly cools, with the areas near the graphite caps losing heat more quickly and ceasing to emit light, while the center of the sample remains glowing white-hot for a longer period. After the optimization process using different configurations the settings for the synthesis of CFC-FG

were set to: $V_{cap} = 175$ V, pulse duration - $t_{pulse} = 200$ ms, and sample resistance $R_{sample} \sim 1 \Omega$. This corresponds to an energy input of 2.5 kJ. The optimized parameters ensured sample preparation with high reproducibility. The flashing process was always continuously

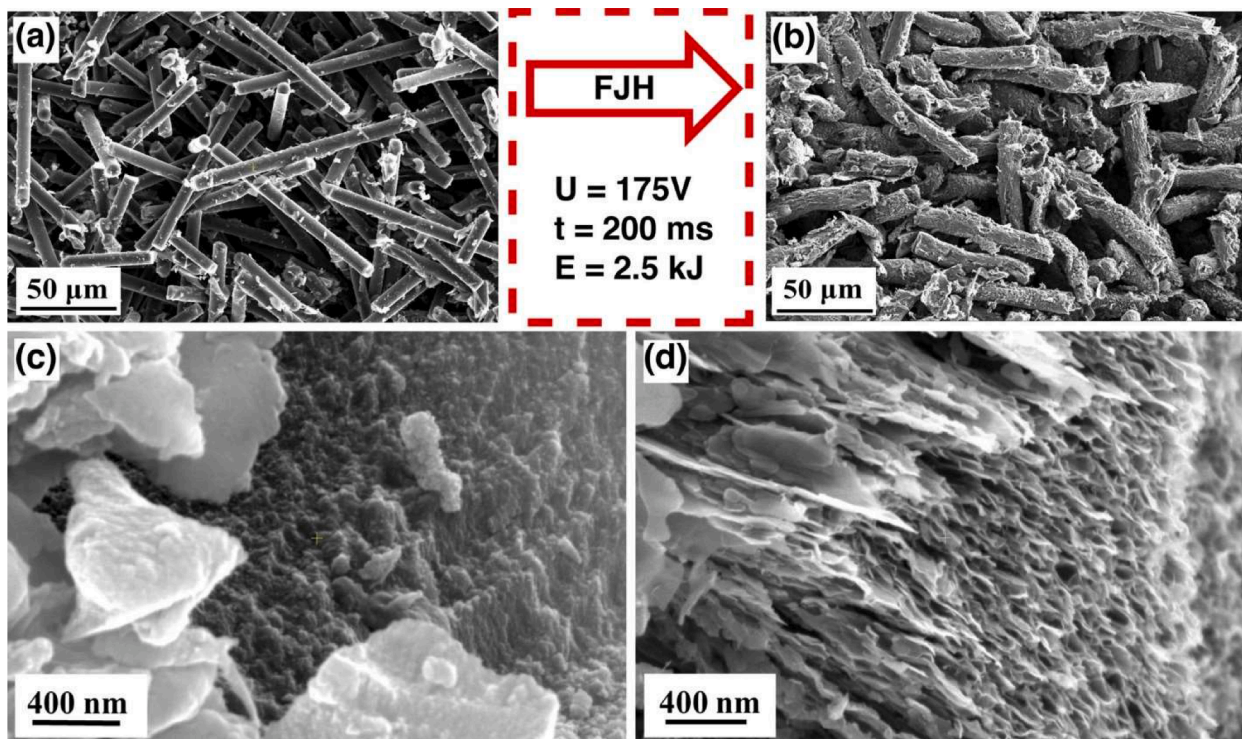


Fig. 2. (a) SEM image of pretreated CFC, (b) SEM image of CFC-FG, (c) High magnification SEM image of pretreated CFC, (d) High magnification SEM image of CFC-FG.

monitored and confirmed by the reliable current and voltage oscillograms **Figure 1(d)** and **Figure 1(e)**. The resulting CFC-FG, which was removed from the glass tube as a single, homogeneous, agglomerated, gray chunk, can be easily crushed with a mortar and pestle. This simplifies the processing of the CFC-FG for subsequent preparation steps.

CFC-FG and pretreated precursor were comprehensively characterized using morphological, spectroscopic, and chemical methods. *Scanning electron microscopy (SEM)* analysis revealed that the pretreatment preserved both the shape and morphology of the carbon fibers. The individual fibers retained their structural integrity and exhibited a smooth surface (**Fig. 2 (a)**). However, the resin matrix was pyrolyzed, resulting in the formation of irregularly shaped particles that adhered to the carbon fibers. While the carbon fibers remained intact, the epoxy resin portion was carbonized. This becomes clearer at higher magnifications (**Fig. 2 (c)**), where the internal structure of a fiber can be seen at the edge of a fracture together with particles of pyrolyzed resin. After FJH, significant changes in the morphology and structure of the CFC-FG can be seen (**Fig. 2 (b)**). Although carbon fibers are known for their high thermal stability, the intense heat generated during flash Joule heating, significantly changed their morphology and porosity. While the original cylindrical shape of the fibers is partially preserved, no fusion or agglomeration takes place. Instead, the fibers develop exfoliated and wrinkled texture with pronounced lamellar macroporosity. At higher magnification (**Fig. 2 (d)**), delaminated graphene multilayers become visible. These layers exhibit multiple well-oriented graphene flake edges, which are known for their excellent catalytic properties due to the altered local electronic structure [39–41]. The layers are loosely packed, with empty spaces between them, which leads to a considerable increase in the porosity and surface area of the material. This was confirmed by the *Gas adsorption/desorption analysis* (**Figure S2**), which shows an increase in specific surface area from $20.7 \text{ m}^2 \text{ g}^{-1}$ to $25.2 \text{ m}^2 \text{ g}^{-1}$. Conversely, the pore volume experiences a notable increase from $0.017570 \text{ cm}^3 \text{ g}^{-1}$ to $0.146406 \text{ cm}^3 \text{ g}^{-1}$. While the increase in surface area

is relatively modest, the substantial rise in pore volume suggests significant structural changes within the material, as corroborated by SEM images. This structural opening, characterized by the expansion or formation of new macropores, enhances accessibility and exposes additional catalytic sites, which could significantly boost the material's catalytic performance. Additionally, *particle size distribution (PSD) analysis* via laser diffraction reveals a narrower PSD for CFC-FG compared to the pretreated precursor. This is accompanied by the disappearance of exceptionally large particles, suggesting delamination and partial disintegration of the carbon fibers, as illustrated in **Figure S3**.

The structural analysis of a lamellar 2D particle on the nanoscale using *transmission electron microscopy (TEM)* revealed a characteristic layered structure (**Fig. 3 (a)**). The number of graphene layers corresponds to multilayer graphene, although some structural defects are evident. These irregularities indicate a turbostratic structure, which is also confirmed by the *selected area electron diffraction (SAED)* of CFC-FG (**Fig. 3 (b)**). The turbostratic character of the prepared CFC-FG is particularly evident from a characteristic feature i.e. the strongly elongated elliptical pattern of the diffraction rings in SAED (see the corresponding given distances for d_{100} in **Fig. 3 (b)**). This phenomenon is due to translational and rotational perturbations as well as the curvature of the graphene sheets with respect to the electron beam. Although such patterns have been reported previously, they are relatively rare [42–44].

To further confirm the turbostratic nature of CFC-FG, an *X-ray diffraction (XRD)* analysis of the CFC-FG powder was performed. According to the literature, the distance between graphene layers in hexagonal graphite (d_{002}) is 0.3354 nm. The XRD pattern for CFC-FG (**Fig. 3 (c)**), revealed a d_{002} of 0.346 nm, confirming the turbostratic structure of CFC-FG. The increased interlayer spacing is a characteristic of turbostratic graphene, where rotational and translational misalignment between layers disrupts the ideal stacking of graphite. This observation is further supported by the asymmetry of the (002) diffraction peak at 2θ

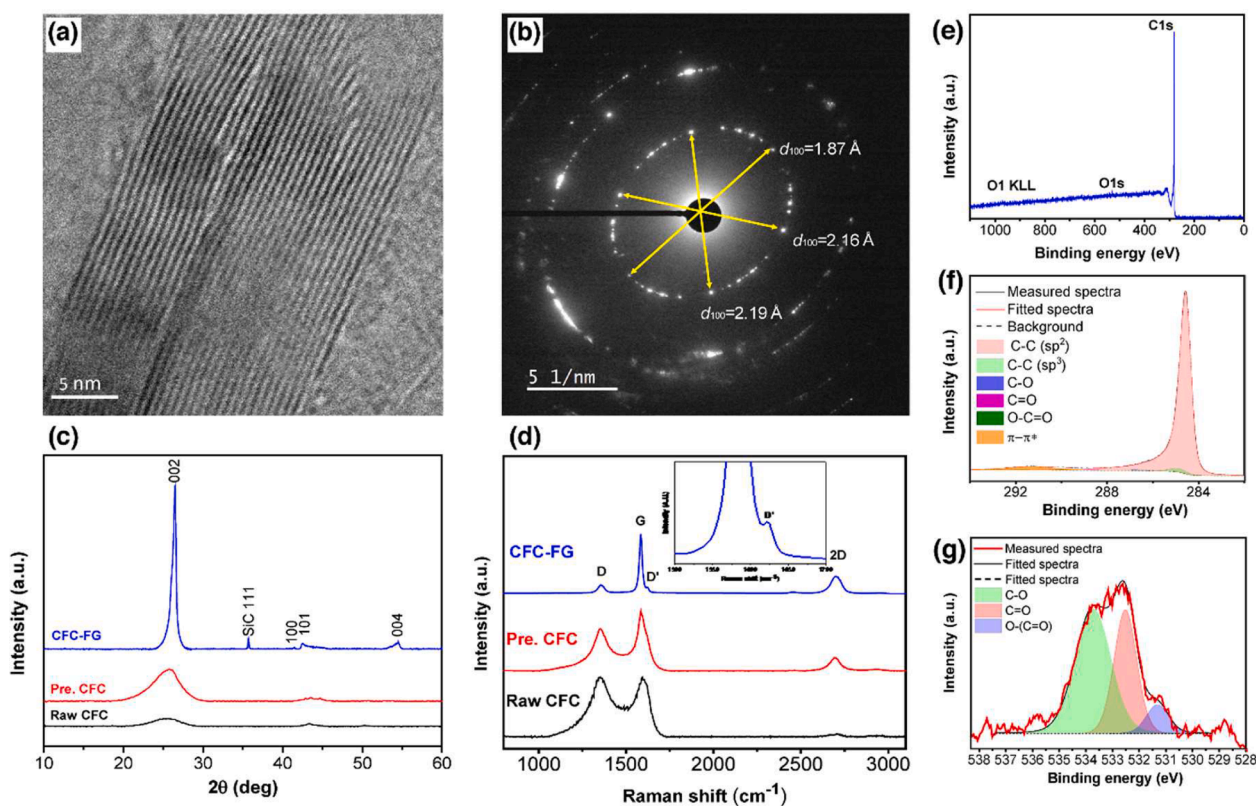


Fig. 3. (a) STEM Bright Field image of CFC-FG, (b) SAED of CFC-FG, (c) XRD of the presented materials, (d) Raman spectra of the presented materials, and (e) XPS survey spectrum of CFC-FG, (f) C 1s core level spectrum of CFC-FG, (g) O 1s core level spectrum of CFC-FG.

26.5°, which exhibits a tail extending toward lower 2θ values. This phenomenon arises from rotational disorder among the individual graphene layers, consistent with findings from previous studies on FG [45]. In contrast, both raw CFC and thermally pretreated CFC showed very broad (002) diffraction peaks, indicating predominantly amorphous structures. The signals observed between 2θ 42° and 45° correspond to the (100) and (101) crystal planes, while the signal at 2θ 54.5° is attributed to the (004) crystal plane. These diffraction peaks are consistent with the structural characteristics of turbostratic graphene materials. Additionally, a peak at 2θ 35.7° indicates the presence of a silicon carbide (SiC) impurity, likely formed in small amounts due to the vaporization of glass from the reaction tube. This underlines the effectiveness of FJH as an energy-efficient method for the graphitization of amorphous carbon materials. By rapidly reaching high temperatures, FJH promotes structural reorganization while avoiding the excessive energy consumption typical of conventional graphitization processes.

Raman spectroscopy analysis was performed for all materials. Given the inhomogeneity of the samples, multiple spectra were recorded, and the averaged spectra are presented in Fig. 3 (d). The Raman analysis confirms the successful upcycling of CFC into flash graphene (CFC-FG), as evidenced by the presence of three prominent peaks: D (~1350 cm^{-1}), G (~1580 cm^{-1}), and 2D (~2700 cm^{-1}). CFC-FG exhibits an $I_{2D/G}$ ratio of 0.3, a common threshold used to identify graphene materials. The D peak, indicative of lattice defects, highlights the defective nature of FG. A particularly noteworthy feature is the distinct D' peak (~1620 cm^{-1}) observed in the inset of Fig. 3 (d). This peak, rarely resolved due to its usual overlap with the G band, has been previously reported [46] and is linked to high defect density in graphene [47,48]. Furthermore, the pronounced D' peak is associated with graphene edges of zigzag configuration, especially in smaller graphene sheets [31]. A single Raman measurement with the highest intensity D' peak from the mapping is shown in Figure S4, further corroborating the production of turbostratic graphene through FJH. These findings emphasize the structural transformations induced by FJH, facilitating the formation of graphene sheets with significant edge defects and confirming the efficient upcycling of CFC into advanced carbon materials.

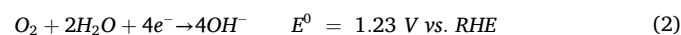
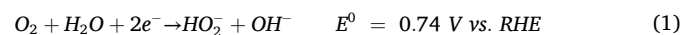
Spectroscopic analysis using X-ray photoelectron spectroscopy (XPS) shows that the synthesis process yields a high-purity product with no detectable impurities during processing. The survey spectrum in Fig. 3 (e) shows mainly carbon, 99.4 at.% and only 0.54 at.% oxygen. Further, high-resolution core level C 1s spectrum in Fig. 3 (f) shows only traces of oxygen-containing functionalities, mainly 91.47 at.% sp^2 carbon (C=C) at binding energy (BE) of 284.5 eV, 2.12 at.% sp^3 carbon (C-C) at BE 284.9 eV, 0.32 at.% hydroxyl or epoxy (C-O) at BE of 286.7 eV, 0.26 at.% carbonyl (C=O) at BE of 288.6 eV, and 0.35 at.% carboxyl (O-C=O) at BE of 289.8 eV. Analysis of the O 1s spectrum (Fig. 3 (g)) corroborates the C 1s spectrum by showing minor contributions from C-O (533.74 eV), C=O (532.5 eV), and O-C(=O) (531.32 eV) functional groups. The extremely low concentration of oxygen functionalities, especially carboxylic groups (-COOH), is favorable for improving the electrochemical stability of the carbon material during the oxygen reduction reaction (ORR), as previously reported [49]. However, the presence of oxygen functionalities can also play a crucial role in improving catalytic activity, especially for the two-electron pathway ($2e^-$ ORR) in the production of hydrogen peroxide (H_2O_2). This dual behavior highlights the trade-off between electrocatalytic selectivity, activity, and stability. The balance between these competing effects is critical when tailoring the material for specific electrochemical applications.

An important property that can significantly influence the material's electrochemical performance at elevated temperatures is also its thermal stability. This was assessed using thermogravimetric analysis (TGA) under dynamic oxidative and inert atmospheres (Figures S5 and S6). In an oxidative atmosphere, CFC-FG exhibits markedly enhanced thermal stability, with a degradation onset temperature of 630 °C, compared to raw CFC and preheated CFC, which display onset temperatures of 300 °C and 525 °C, respectively. The elevated degradation temperature of CFC-

FG suggests a high degree of structural integrity and resistance to oxidation, attributed to its improved graphitization. This is consistent with findings from complementary characterization techniques, including SAED, XRD, and Raman spectroscopy, which confirm the high graphitic content and turbostratic structure of the material. The enhanced thermal stability also implies potential electrochemical stability under elevated temperature conditions, a desirable feature for various high-performance applications such as fuel cells, supercapacitors, and other electrocatalytic processes including H_2O_2 electrosynthesis. Thermal stability, combined with the structural and compositional properties of CFC-FG, highlights its suitability for demanding electrochemical environments.

3.2. Electrochemical characterization

The oxygen reduction reaction (ORR) activity, selectivity, and stability of CFC-FG for H_2O_2 electrosynthesis were systematically evaluated using electrochemical techniques. As previously reported, carbon materials exhibit high selectivity for the $2e^-$ ORR pathway, which favors the formation of hydrogen peroxide in alkaline electrolytes. Accordingly, all measurements were performed in 0.1 M KOH. The competing, undesired $4e^-$ ORR pathway leads to the formation of water (H_2O), as shown in Eqs. (1) and (2). It is important to note that the pK_a value of H_2O_2 is 11.6, which means that hydrogen peroxide in 0.1 M KOH is predominantly in its deprotonated form, HO_2^- [50].



To benchmark the activity, selectivity, and stability of synthesized CFC-FG for $2e^-$ ORR, we chose glassy carbon (GC) and highly oriented pyrolytic graphite (HOPG) for comparison. This choice is based on the different structural properties of these materials. HOPG surfaces are highly crystalline with a graphitic character and minimal defects, while GC surfaces are amorphous or non-graphitic and have a higher density of structural defects. Turbostratic graphene, such as CFC-FG, uniquely combines the properties of both materials. As explained in the previous chapter, CFC-FG exhibits a turbostratic graphitic nature alongside a significant concentration of structural defects. In addition, unlike pure graphene, CFC-FG contains a low concentration of oxygen functionalities that are known to increase the catalytic activity for the oxygen reduction reaction (ORR) [51]. Fig. 4 (a) shows the ORR polarization curves measured in 0.1 M KOH electrolyte (pH ~ 13) for each electrocatalyst at the disk electrode, along with the simultaneous detection of hydrogen peroxide (H_2O_2) species at the ring electrode. The ORR polarization curves clearly show that CFC-FG has the highest current density and the lowest overpotential among the electrocatalysts, followed by GC and HOPG, e.g. 50 mV and 140 mV lower at -0.1 mA cm^{-2} than GC and HOPG, respectively. The high activity presented by CFC-FG reflects its relatively high surface area when the current values are normalized by the geometrical surface area (mA cm^{-2}).

To evaluate the electrocatalytic activity of the individual catalyst, kinetic current (i_k) was first obtained from measured current (i) using Koutecky-Levich equation (Equation S3 in the Supplementary Materials) [52,53]. i_k was normalized by the electrochemical surface area (ECSA, $\text{cm}^2_{\text{real}}$) to obtain intrinsic activities of the catalysts (j_k [$\text{mA cm}^{-2}_{\text{real}}$]). ECSA for each electrocatalyst was determined using the capacitance method (Equation S1 and Figure S8 in the Supplementary Materials), where the electrochemical double layer capacitance (C_{dl}) values were extracted from current vs. scan rate plots (Figure S7 in the Supplementary Materials). ECSA was then obtained by dividing the C_{dl} with the specific capacitance (C_s) of a flat standard electrode, reported as $40 \mu\text{F cm}^{-2}_{\text{real}}$ [54-56] (refer to the Supplementary Materials for further details). For visualization, we plotted Tafel plots (E vs. j_k) for each electrocatalyst (Fig. 4 (b)). The results show that GC has a slightly higher

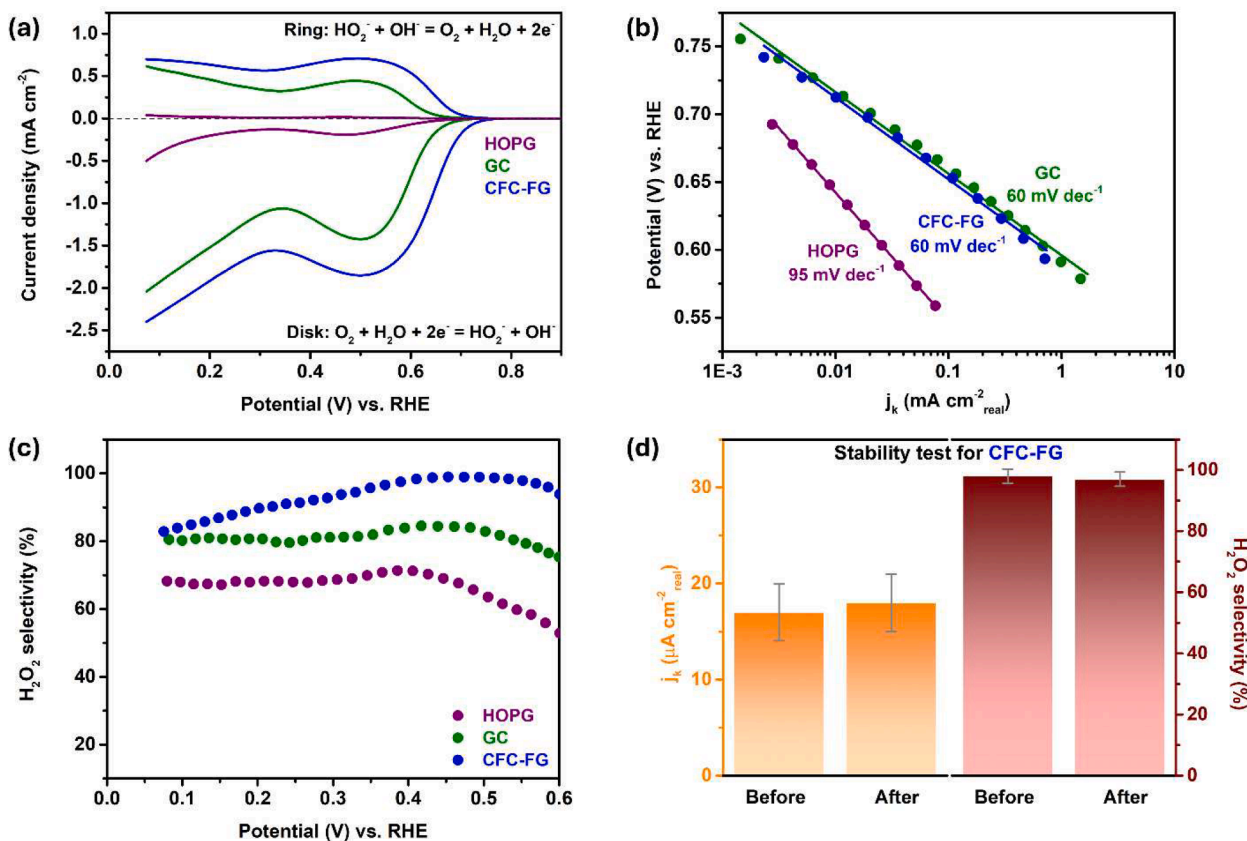


Fig. 4. Electrochemical evaluation of electrocatalysts via RRDE. (a) Polarization curves for the oxygen reduction reaction (ORR) and the simultaneous detection of hydrogen peroxide species (HO₂⁻ in alkaline media) measured at the disk and the ring electrodes, respectively. The curves were measured in 0.1 M KOH electrolyte saturated with oxygen at 50 mV s⁻¹ and a rotation speed of 1600 rpm. The polarization is in the cathodic direction (i.e., “negative going” sweep). (b) Tafel plots and their respective Tafel slopes and (c) corresponding selectivity for H₂O₂ electrosynthesis, determined from the ORR polarization curves for each electrocatalyst shown in (a). (d) Activity (j_k value at $E = 0.7$ V vs RHE) and selectivity (at $E = 0.55$ V vs RHE) for the H₂O₂ electrosynthesis before and after the stability test for the CFC-FG electrocatalyst. The stability test was performed in 0.1 M KOH electrolyte saturated with oxygen, at a rotation speed of 1600 rpm, by applying a potential of 0.55 V vs. RHE for a period of 25 hours. Refer to the experimental section for further details.

intrinsic activity than CFC-FG, with HOPG having the lowest ORR activity. In fact, the GC surface is reported in the literature as one of the most active surfaces for H₂O₂ electrosynthesis by ORR in alkaline media [50]. The similar Tafel slopes for GC and CFC-FG suggest that the 2e⁻ ORR follows the same reaction mechanism on both surfaces. Although the intrinsic activities of GC and CFC-FG are similar, the latter offers significant advantages over GC in practical electrochemical systems for H₂O₂ production. Its porous structure provides good access for the dissolved O₂, while the more compact GC structure has only a surface with closed porosity. Further, the great catalytic properties of the CFC-FG can be referred to the observed defect-rich and highly disordered structure of this material. Defects within the graphene lattice and along plane edges are well-documented for their catalytic influence on the electrochemical synthesis of H₂O₂. Chen et al. demonstrated that sp²-type defects can act as active sites for the 2e⁻ ORR [12]. In addition, it was shown previously that FJH derived graphene materials retain excellent electrical conductivity, which enables efficient charge transfer during electrochemical reactions [29]. This could lead to higher overall efficiency and lower power consumption in practical systems.

To quantify the selectivity, the amount of H₂O₂ generated during ORR was determined by the ratio of the current measured at the ring (corrected for the collection efficiency, N) to the current measured at the disk electrode (Equation S2 in the Supplementary Materials). Calculated selectivity in the potential range is presented in Fig. 4 (c). It is evident that CFC-FG has a superior H₂O₂ selectivity (close to 100 % at a potential range from 0.55 to 0.25 V vs. RHE), compared to GC and HOPG (around 80 % and 70 % selectivity, respectively). Additionally, the

selectivity of CFC-FG surpasses that of previously published carbon-based (non-metal) electrocatalysts, which have demonstrated selectivity ranging from 60 % to 95 % [9–14]. The near-maximum selectivity of CFC-FG can be attributed to its distinct combination of properties, including a high concentration of defects, the presence of oxygen functionalities on the surface, and rotational disorder or misalignment between graphene sheets, which increases interlayer spacing in turbostratic graphene. As demonstrated by density functional theory (DFT) simulations, a variety of defects in model graphene systems are likely to exhibit selectivity for the 2e⁻ ORR [12]. Notably, the D' band, observed to be particularly intense in CFC-FG (Fig. 3 (c)), is associated with the partial oxidation of sp² basal plane carbon in graphene-based materials. These sites have been shown to interact effectively with intermediates involved in H₂O₂ formation, thereby contributing to exceptional activity and selectivity in carbon-based catalysts [57,58]. These features, as well as other potential synergistic interactions, likely contribute to the material's prominent catalytic activity for the 2e⁻ ORR. We also recognize that the structural features responsible for the prominent D'-peak and the elliptical SAED pattern, both rarely observed in carbon-based materials, may influence the catalytic properties. However, the exact role of these features on ORR performance is still largely unexplored and is the focus of our follow-up study.

As discussed above, high activity and selectivity are two essential prerequisites for an energy-efficient electrocatalyst. Another crucial requirement for practical electrocatalyst material is that it must possess good stability. To evaluate and compare the stability of CFC-FG, the stability test was conducted by applying a potential of 0.55 V (vs. RHE)

for a period of 25 hours under the same conditions (refer to the Supplementary Materials for further details). This potential was chosen for one main reason: it is the lowest overpotential (Fig. 4 (a)) at which the selectivity for H₂O₂ is close to 100 % (Fig. 4 (c)). Fig. 4 (d) shows a comparison of the activity and selectivity for H₂O₂ electrosynthesis with the CFC-FG electrocatalyst before and after the stability test. CFC-FG showed good activity and selectivity, which remained essentially unchanged. The stable intrinsic activity of CFC-FG suggests that its surface is unsusceptible to significant chemical and structural changes during operating conditions for H₂O₂ electrosynthesis. Moreover, the observed high stability can likely be attributed to its turbostratic graphitic structure, a thermodynamically stable carbon allotrope. Consequently, the results of the degradation test highlight the promising performance of the synthesized CFC-FG and underscore its suitability for H₂O₂ electrosynthesis application.

4. Conclusions

Flash Joule heating has proven to be a highly effective method for upcycling used or expired carbon fiber composites (CFC) into turbostratic flash graphene (FG), solving the challenges associated with existing bulk graphene synthesis methods. This innovative approach utilizes a tailored setup that is characterized by its simplicity and scalability, making it ideally suited for recycling and upcycling of CFC. Characterization studies show that the synthesized CFC-derived flash graphene (CFC-FG) retains the tubular morphology of its precursor while exhibiting a high pore volume and significant specific surface area. In addition, oxygen functional groups have been identified to provide the material with valuable chemical versatility. CFC-FG exhibits a unique defect-rich turbostratic structure as evidenced by the distinct D' peak in Raman spectra and the elliptical ring patterns in electron diffraction (SAED). These characteristic morphological, structural, and chemical properties contribute to its sound catalytic performance in the two-electron oxygen reduction reaction (2e⁻ ORR). The material achieves nearly 100 % selectivity for hydrogen peroxide (H₂O₂) electrosynthesis and exhibits modest catalytic activity. Its highly graphitic nature not only increases stability but also ensures a long lifetime, making it well-suited for demanding electrochemical environments. While its activity is comparable to that of glassy carbon (GC), CFC-FG offers greater functional versatility. A key advantage of turbostratic FG is its sustainability. It is obtained from low-value waste materials in a solvent-free, acid-free process and represents an environmentally friendly alternative to conventional methods. The straightforward, robust synthesis process is in line with green chemistry principles, reduces environmental impact, and improves the overall sustainability profile. The promising catalytic efficiency of FG combined with favorable techno-economic considerations also makes it a viable candidate for sustainable and efficient H₂O₂ production.

Apart from the sustainable electrocatalytic capabilities, this method offers significant environmental benefits by converting waste into high-value materials. This innovative upcycling approach not only advances materials science but also highlights the critical role of sustainable practices in addressing environmental challenges.

CRedit authorship contribution statement

Ivo Bardarov: Writing – original draft, Investigation, Formal analysis, Data curation, Conceptualization. **Desislava Yordanova Apostolova:** Writing – original draft, Visualization, Investigation. **Pedro Martins:** Writing – original draft, Investigation, Formal analysis, Data curation. **Ivo Angelov:** Supervision, Conceptualization. **Francisco Ruiz-Zepeda:** Investigation. **Ivan Jerman:** Supervision, Investigation. **Matevž Dular:** Investigation. **Dušan Strmcnik:** Writing – review & editing, Supervision, Funding acquisition, Data curation. **Boštjan Genorio:** Writing – review & editing, Writing – original draft, Supervision, Resources, Project administration, Methodology, Investigation, Funding

acquisition, Formal analysis, Data curation, Conceptualization.

Declaration of competing interest

The authors declare that they have no known competing financial interests or personal relationships that could have appeared to influence the work reported in this paper.

Acknowledgments

The financial support of the Slovenian Research and Innovation Agency (ARIS) through grants P2-0423, P1-0447, J7-4636, J2-50086, and J7-50227 is gratefully acknowledged.

Supplementary materials

Supplementary material associated with this article can be found, in the online version, at doi:10.1016/j.electacta.2025.145754.

Data availability

Data will be made available on request.

References

- [1] Y. Wen, Y. Feng, J. Wei, T. Zhang, C. Cai, J. Sun, X. Qian, Y. Zhao, Photovoltaic-driven stable electrosynthesis of H₂O₂ in simulated seawater and its disinfection application, *Chem. Sci.* 15 (2024) 18969–18976, <https://doi.org/10.1039/D4SC05909C>.
- [2] J.M. Campos-Martin, G. Blanco-Brieva, J.L.G. Fierro, Hydrogen peroxide synthesis: an outlook beyond the anthraquinone process, *Angew. Chem. Int Ed* 45 (2006) 6962–6984, <https://doi.org/10.1002/anie.200503779>.
- [3] P. Farinazzo Bergamo Dias Martins, I. Plazl, D. Strmcnik, B. Genorio, Prospect of microfluidic devices for on-site electrochemical production of hydrogen peroxide, *Curr. Opin. Electrochem.* 38 (2023) 101223, <https://doi.org/10.1016/j.coelec.2023.101223>.
- [4] A. Verdager-Casadevall, D. Deiana, M. Karamad, S. Siahrostami, P. Malacrida, T. W. Hansen, J. Rossmel, I. Chorkendorff, I.E.L. Stephens, Trends in the electrochemical synthesis of H₂O₂: enhancing activity and selectivity by electrocatalytic site engineering, *Nano Lett.* 14 (2014) 1603–1608, <https://doi.org/10.1021/nl500037x>.
- [5] E. Pizzutillo, O. Kasian, C.H. Choi, S. Cherevko, G.J. Hutchings, K.J.J. Mayrhofer, S. J. Freakley, Electrocatalytic synthesis of hydrogen peroxide on Au-Pd nanoparticles: From fundamentals to continuous production, *Chem. Phys. Lett.* 683 (2017) 436–442, <https://doi.org/10.1016/j.cplett.2017.01.071>.
- [6] X. Cui, L. Zhong, X. Zhao, J. Xie, D. He, X. Yang, K. Lin, H. Wang, L. Niu, Ultrafine Co nanoparticles confined in nitrogen-doped carbon toward two-electron oxygen reduction reaction for H₂O₂ electrosynthesis in acidic media, *Chin. Chem. Lett.* 34 (2023) 108291, <https://doi.org/10.1016/j.ccllet.2023.108291>.
- [7] Q. Zhang, L. Zheng, F. Gu, J. Wu, J. Gao, Y.-C. Zhang, X.-D. Zhu, Recent advances in single-atom catalysts for acidic electrochemical oxygen reduction to hydrogen peroxide, *Nano Energy* 116 (2023) 108798, <https://doi.org/10.1016/j.nanoen.2023.108798>.
- [8] M. Nosan, D. Strmcnik, V. Brusko, M. Kirsanova, M. Finšgar, A.M. Dimiev, B. Genorio, Correlating nickel functionalities to selectivity for hydrogen peroxide electrosynthesis, *Sustain. Energy Fuels* 7 (2023) 2270–2278, <https://doi.org/10.1039/D3SE00139C>.
- [9] Z. Lu, G. Chen, S. Siahrostami, Z. Chen, K. Liu, J. Xie, L. Liao, T. Wu, D. Lin, Y. Liu, T.F. Jaramillo, J.K. Nørskov, Y. Cui, High-efficiency oxygen reduction to hydrogen peroxide catalysed by oxidized carbon materials, *Nat. Catal.* 1 (2018) 156–162, <https://doi.org/10.1038/s41929-017-0017-x>.
- [10] X. Hu, X. Zeng, Y. Liu, J. Lu, X. Zhang, Carbon-based materials for photo- and electrocatalytic synthesis of hydrogen peroxide, *Nanoscale* 12 (2020) 16008–16027, <https://doi.org/10.1039/D0NR03178J>.
- [11] X. Wang, Y. Liu, Z. Liu, Z. Li, T. Zhang, Y. Cheng, L. Lei, B. Yang, Y. Hou, Highly efficient electrosynthesis of H₂O₂ in acidic electrolyte on metal-free heteroatoms co-doped carbon nanosheets and simultaneously promoting Fenton process, *Chin. Chem. Lett.* 35 (2024) 108926, <https://doi.org/10.1016/j.ccllet.2023.108926>.
- [12] S. Chen, Z. Chen, S. Siahrostami, T.R. Kim, D. Nordlund, D. Sokaras, S. Nowak, J. W.F. To, D. Higgins, R. Sinclair, J.K. Nørskov, T.F. Jaramillo, Z. Bao, Defective carbon-based materials for the electrochemical synthesis of hydrogen peroxide, *ACS Sustain. Chem. Eng.* 6 (2018) 311–317, <https://doi.org/10.1021/acssuschemeng.7b02517>.
- [13] V. Perazzolo, C. Durante, R. Pilot, A. Paduano, J. Zheng, G.A. Rizzi, A. Martucci, G. Granozzi, A. Gennaro, Nitrogen and sulfur doped mesoporous carbon as metal-free electrocatalysts for the in situ production of hydrogen peroxide, *Carbon*. N. Y. 95 (2015) 949–963, <https://doi.org/10.1016/j.carbon.2015.09.002>.

- [14] Z. Sang, F. Hou, S. Wang, J. Liang, Research progress on carbon-based non-metallic nanomaterials as catalysts for the two-electron oxygen reduction for hydrogen peroxide production, *New Carbon Mater.* 37 (2022) 136–151, [https://doi.org/10.1016/S1872-5805\(22\)60583-3](https://doi.org/10.1016/S1872-5805(22)60583-3).
- [15] J. Zhang, G. Lin, U. Vaidya, H. Wang, Past, present and future prospective of global carbon fibre composite developments and applications, *Compos. Part B* 250 (2023) 110463, <https://doi.org/10.1016/j.compositesb.2022.110463>.
- [16] N.M. Akash, S. Saad, M.A.A. Bari, R. Sarker, C. Gupta, G. Asghari Sarabi, A. Phani, F. Zahin, S. Tabassum, K. Subramanian, S. Kim, M.M. Rahman, P. Egberts, M. G. Kibria, Development of asphaltene-derived carbon fiber reinforced composites via additive manufacturing, *Carbon*. N. Y. 228 (2024) 119413, <https://doi.org/10.1016/j.carbon.2024.119413>.
- [17] J. Qureshi, A review of recycling methods for fibre reinforced polymer composites, *Sustainability*. 14 (2022) 16855, <https://doi.org/10.3390/su142416855>.
- [18] A. Danish, M.A. Mosaberpanah, M.U. Salim, M. Amran, R. Fediuk, T. Ozbakkaloglu, M.F. Rashid, Utilization of recycled carbon fiber reinforced polymer in cementitious composites: A critical review, *J. Build. Eng.* 53 (2022) 104583, <https://doi.org/10.1016/J.JOBE.2022.104583>.
- [19] S. Pimenta, S.T. Pinho, Recycling carbon fibre reinforced polymers for structural applications: Technology review and market outlook, *Waste Manag.* 31 (2011) 378–392, <https://doi.org/10.1016/j.wasman.2010.09.019>.
- [20] E. Pakdel, S. Kashi, R. Varley, X. Wang, Recent progress in recycling carbon fibre reinforced composites and dry carbon fibre wastes, *Resources, Conservation and Recycling* 166 (2021) 105340, <https://doi.org/10.1016/J.RESCONREC.2020.105340>.
- [21] S.J. Pickering, Recycling technologies for thermoset composite materials—current status, *Appl. Sci. Manufact.* 37 (2006) 1206–1215, <https://doi.org/10.1016/J.COMPOSITESA.2005.05.030>.
- [22] J.A. Butenegro, M. Bahrami, J. Abenojar, M.Á. Martínez, Recent progress in carbon fiber reinforced polymers recycling: a review of recycling methods and reuse of carbon fibers, *Materials* 14 (2021) 6401, <https://doi.org/10.3390/ma14216401>.
- [23] D. Borjan, Ž. Knez, M. Knez, Recycling of carbon fiber-reinforced composites—difficulties and future perspectives, *Materials*. (Basel) 14 (2021), <https://doi.org/10.3390/MA14154191>.
- [24] J. Zhang, V.S. Chevali, H. Wang, C.H. Wang, Current status of carbon fibre and carbon fibre composites recycling, *Compos. Part B* 193 (2020) 108053, <https://doi.org/10.1016/J.COMPOSITESB.2020.108053>.
- [25] M.Y. Khalid, Z.U. Arif, W. Ahmed, H. Arshad, Recent trends in recycling and reusing techniques of different plastic polymers and their composite materials, *Sustain. Mater. Techn.* 31 (2022) e00382, <https://doi.org/10.1016/J.SUSMAT.2021.E00382>.
- [26] C. Wang, H. Geng, R. Sun, H. Song, Technological potential analysis and vacant technology forecasting in the graphene field based on the patent data mining, *Resour. Policy*. 77 (2022) 102636, <https://doi.org/10.1016/J.RESOURPOL.2022.102636>.
- [27] S.K. Tiwari, S. Sahoo, N. Wang, A. Huczko, Graphene research and their outputs: Status and prospect, *Adv. Mater. Dev.* 5 (2020) 10–29, <https://doi.org/10.1016/J.JSAMD.2020.01.006>.
- [28] K.M. Wyss, J.L. Beckham, W. Chen, D.X. Luong, P. Hundi, S. Raghuraman, R. Shahsavari, J.M. Tour, Converting plastic waste pyrolysis ash into flash graphene, *Carbon*. N. Y. 174 (2021) 430–438, <https://doi.org/10.1016/J.CARBON.2020.12.063>.
- [29] D.X. Luong, K.V. Bets, W.A. Algozeeb, M.G. Stanford, C. Kittrell, W. Chen, R. V. Salvatierra, M. Ren, E.A. McHugh, P.A. Advincula, Z. Wang, M. Bhatt, H. Guo, V. Mancevski, R. Shahsavari, B.I. Yakobson, J.M. Tour, Gram-scale bottom-up flash graphene synthesis, *Nature* 577 (2020) 647–651, <https://doi.org/10.1038/s41586-020-1938-0>.
- [30] B. Deng, Z. Wang, C.H. Choi, G. Li, Z. Yuan, J. Chen, D.X. Luong, L. Eddy, B. Shin, A. Latham, W. Chen, Y. Cheng, S. Xu, Q. Liu, Y. Han, B.I. Yakobson, Y. Zhao, J. M. Tour, Kinetically controlled synthesis of metallic glass nanoparticles with expanded composition space, *Adv. Mater.* 36 (2024) 2309956, <https://doi.org/10.1002/adma.202309956>.
- [31] K.M. Wyss, Z. Wang, L.B. Alemany, C. Kittrell, J.M. Tour, Bulk production of any ratio ¹²C:¹³C turbostratic flash graphene and its unusual spectroscopic characteristics, *ACS. Nano* 15 (2021) 10542–10552, <https://doi.org/10.1021/acsnano.1c03197>.
- [32] K.M. Wyss, W. Chen, J.L. Beckham, P.E. Savas, J.M. Tour, Holey and wrinkled flash graphene from mixed plastic waste, *ACS. Nano* 16 (2022) 7804–7815, <https://doi.org/10.1021/acsnano.2c00379>.
- [33] I. Bardarov, D.Y. Apostolova, M.M. Mathew, M. Nosan, P.F.B.D. Martins, B. Genorio, Flash graphene: a sustainable prospect for electrocatalysis, *Acta Chim. Slov.* 71 (2024) 541–557, <https://doi.org/10.17344/acsi.2024.8794>.
- [34] W. Chen, C. Ge, J.T. Li, J.L. Beckham, Z. Yuan, K.M. Wyss, P.A. Advincula, L. Eddy, C. Kittrell, J. Chen, D.X. Luong, R.A. Carter, J.M. Tour, Heteroatom-doped flash graphene, *ACS. Nano* 16 (2022) 6646–6656, <https://doi.org/10.1021/acsnano.2c01136>.
- [35] B. Deng, D.X. Luong, Z. Wang, C. Kittrell, E.A. McHugh, J.M. Tour, Urban mining by flash Joule heating, *Nat. Commun.* 12 (2021) 5794, <https://doi.org/10.1038/s41467-021-26038-9>.
- [36] K.S. Ravi Chandran, Transient Joule heating of graphene, nanowires and filaments: Analytical model for current-induced temperature evolution including substrate and end effects, *Int. J. Heat. Mass Transf.* 88 (2015) 14–19, <https://doi.org/10.1016/j.ijheatmasstransfer.2015.04.014>.
- [37] L. Sun, X. Wu, Y. Jiao, C. Jia, T. Teng, L. Lin, F. Yu, Z. He, J. Gao, S. Yan, G. Shi, Z. J. Ren, J. Yang, S. Zhang, X. Zhu, Millisecond self-heating and quenching synthesis of Fe/carbon nanocomposite for superior reductive remediation, *Appl. Catal. B* 342 (2024) 123361, <https://doi.org/10.1016/j.apcatb.2023.123361>.
- [38] P. Huang, R. Zhu, X. Zhang, W. Zhang, Effect of free radicals and electric field on preparation of coal pitch-derived graphene using flash Joule heating, *Chem. Eng. J.* 450 (2022) 137999, <https://doi.org/10.1016/j.cej.2022.137999>.
- [39] K. Jiang, J. Zhao, H. Wang, Catalyst design for electrochemical oxygen reduction toward hydrogen peroxide, *Adv. Funct. Mater.* 30 (2020) 2003321, <https://doi.org/10.1002/adfm.202003321>.
- [40] A. Shen, Y. Zou, Q. Wang, R.A.W. Dryfe, X. Huang, S. Dou, L. Dai, S. Wang, Oxygen reduction reaction in a droplet on graphite: direct evidence that the edge is more active than the basal plane, *Angew. Chem. Int Ed* 53 (2014) 10804–10808, <https://doi.org/10.1002/anie.201406695>.
- [41] D. Yan, Y. Li, J. Huo, R. Chen, L. Dai, S. Wang, Defect chemistry of nonprecious-metal electrocatalysts for oxygen reactions, *Adv. Mater.* 29 (2017) 1606459, <https://doi.org/10.1002/adma.201606459>.
- [42] C. Binder, T. Bendo, G. Hammes, G.O. Neves, R. Binder, J.D.B. de Mello, A.N. Klein, Structure and properties of in situ-generated two-dimensional turbostratic graphite nodules, *Carbon*. N. Y. 124 (2017) 685–692, <https://doi.org/10.1016/j.carbon.2017.09.036>.
- [43] M. Seyring, A. Simon, I. Voigt, U. Ritter, M. Rettenmayr, Quantitative crystallographic analysis of individual carbon nanofibers using high resolution transmission electron microscopy and electron diffraction, *Carbon*. N. Y. 116 (2017) 347–355, <https://doi.org/10.1016/j.carbon.2017.01.107>.
- [44] M. Singh, A. Sengupta, K. Zeller, G. Skoptsov, R.L. Vander Wal, Effect of hydrogen concentration on graphene synthesis using microwave-driven plasma-mediated methane cracking, *Carbon*. N. Y. 143 (2019) 802–813, <https://doi.org/10.1016/j.carbon.2018.11.082>.
- [45] M.A.S.R. Saadi, P.A. Advincula, M.S.H. Thakur, A.Z. Khater, S. Saad, A. Shayesteh Zeraati, S.K. Nabil, A. Zinke, S. Roy, M. Lou, S.N. Bheemasetti, M.A.A. Bari, Y. Zheng, J.L. Beckham, V. Gadhamsetty, A. Vashisth, M.G. Kibria, J.M. Tour, P. M. Ajayan, M.M. Rahman, Sustainable valorization of asphaltene via flash joule heating, *Sci. Adv.* 8 (2022) eadd3555, <https://doi.org/10.1126/sciadv.add3555>.
- [46] K.M. Wyss, D.X. Luong, J.M. Tour, Large-Scale syntheses of 2D materials: flash joule heating and other methods, *Adv. Mater.* 34 (2022) 2106970, <https://doi.org/10.1002/adma.202106970>.
- [47] A. Sacco, C. Portesi, A.M. Giovannozzi, A.M. Rossi, Graphene edge method for three-dimensional probing of Raman microscopes focal volumes, *J. Raman Spectrosc.* 52 (2021) 1671–1684, <https://doi.org/10.1002/jrs.6187>.
- [48] L.G. Cañado, A. Jorio, M.A. Pimenta, Measuring the absolute Raman cross section of nanographites as a function of laser energy and crystallite size, *Phys. Rev. B* 76 (2007) 064304, <https://doi.org/10.1103/PhysRevB.76.064304>.
- [49] L. Pavko, M. Gatalo, T. Dukić, F. Ruiz-Zepeda, A.K. Surca, M. Šala, N. Maselj, P. Jovanović, M. Bele, M. Finšgar, B. Genorio, N. Hodnik, M. Gaberšček, Correlating oxygen functionalities and electrochemical durability of carbon supports for electrocatalysts, *Carbon*. N. Y. 215 (2023) 118458, <https://doi.org/10.1016/j.carbon.2023.118458>.
- [50] S. Yang, A. Verdager-Casadevall, L. Arnarson, L. Silvioli, V. Čolić, R. Frydendal, J. Rossmel, I. Chorkendorff, I.E.L. Stephens, Toward the decentralized electrochemical production of H₂O₂: a focus on the catalysis, *ACS. Catal.* 8 (2018) 4064–4081, <https://doi.org/10.1021/acscatal.8b00217>.
- [51] C.-X. Zhao, B.-Q. Li, Q. Zhang, Advanced electrosynthesis of hydrogen peroxide on oxidized carbon electrocatalyst, *J. Energy Chem.* 34 (2019) 10–11, <https://doi.org/10.1016/j.jechem.2018.09.002>.
- [52] N. Markovic, Surface science studies of model fuel cell electrocatalysts, *Surf. Sci. Rep.* 45 (2002) 117–229, [https://doi.org/10.1016/S0167-5729\(01\)00022-X](https://doi.org/10.1016/S0167-5729(01)00022-X).
- [53] K.J.J. Mayrhofer, D. Strmcnik, B.B. Bliznac, V. Stamenkovic, M. Arenz, N. M. Markovic, Measurement of oxygen reduction activities via the rotating disc electrode method: From Pt model surfaces to carbon-supported high surface area catalysts, *Electrochim. Acta* 53 (2008) 3181–3188, <https://doi.org/10.1016/j.electacta.2007.11.057>.
- [54] C. Zhang, J. Sha, H. Fei, M. Liu, S. Yazdi, J. Zhang, Q. Zhong, X. Zou, N. Zhao, H. Yu, Z. Jiang, E. Ringe, B.I. Yakobson, J. Dong, D. Chen, J.M. Tour, Single-atomic ruthenium catalytic sites on nitrogen-doped graphene for oxygen reduction reaction in acidic medium, *ACS. Nano* 11 (2017) 6930–6941, <https://doi.org/10.1021/acsnano.7b02148>.
- [55] J. Zhang, M. Ren, L. Wang, Y. Li, B.I. Yakobson, J.M. Tour, Oxidized laser-induced graphene for efficient oxygen electrocatalysis, *Adv. Mater.* 30 (2018) 1707319, <https://doi.org/10.1002/adma.201707319>.
- [56] Z. Wang, Q.-K. Li, C. Zhang, Z. Cheng, W. Chen, E.A. McHugh, R.A. Carter, B. I. Yakobson, J.M. Tour, Hydrogen Peroxide Generation with 100% Faradaic efficiency on metal-free carbon black, *ACS. Catal.* 11 (2021) 2454–2459, <https://doi.org/10.1021/acscatal.0c04735>.
- [57] W. Wang, Y. Zheng, Y. Hu, Y. Liu, S. Chen, Intrinsic carbon defects for the electrosynthesis of H₂O₂, *J. Phys. Chem. Lett.* 13 (2022) 8914–8920, <https://doi.org/10.1021/acs.jpclett.2c02684>.
- [58] H.W. Kim, M.B. Ross, N. Kormienko, L. Zhang, J. Guo, P. Yang, B.D. McCloskey, Efficient hydrogen peroxide generation using reduced graphene oxide-based oxygen reduction electrocatalysts, *Nat. Catal.* 1 (2018) 282–290, <https://doi.org/10.1038/s41929-018-0044-2>.